Wave energy conversion using coupled balloons: A numerical investigation

Bo-Lin Chen, Adi Kurniawan, Hugh Wolgamot, and James R. Whelan

***Abstract*—Most wave energy converters (WECs) feature rigid structures, while flexible WECs have received less attention. This study investigates a novel WEC comprising two balloons coupled through an air duct, designed as a simple and low-cost solution for harnessing wave energy. The performance of the coupled balloon wave energy converter (CBWEC) is assessed through simplified linear numerical modelling, using the radiation/diffraction software HydroStar. The balloons are idealised as spheres with uniform deformation. A comprehensive parametric study evaluates the device's performance with varying spacing, submergence, power take-off damping, and additional stiffness. Although the CBWEC was initially conceived as fully submerged, results indicate that without additional negative stiffness, its natural period is too low to resonate with ocean waves. Hence, in the absence of negative stiffness, a floating configuration offers the highest potential power, defined as the area under the power function. Hypothetically introducing negative stiffness significantly improves performance, producing five times more power than the best configuration without it. With appropriate negative stiffness, the submergence of the balloons becomes less critical. These findings will guide upcoming physical experiments to validate the proposed device. While achieving negative stiffness may be challenging in practice, the CBWEC demonstrates reasonable performance even without it, highlighting its potential as a promising WEC.**

***Index Terms*—Flexible wave energy converter, pressure differential, negative stiffness, numerical modelling**

I. Introduction

THIS paper considers a wave energy device in the form of two air-filled balloons connected by a pipe, hereafter referred to as the coupled balloon wave energy converter (CBWEC). A concept sketch is presented in Fig. 1. The balloons are tethered to the seabed and spaced approximately half a wavelength apart along the direction of wave propagation. When subjected to wave action, the balloons alternately contract and expand, pumping air back and forth between them. This airflow can be used to drive a turbine. In storm conditions, the balloons may be deflated and stored on the seabed.

The concept is potentially attractive due to its very low capital cost, resulting from low material and installation requirements.

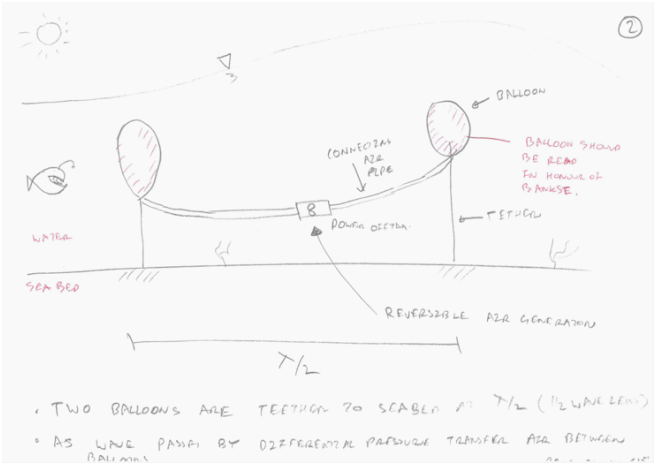

Fig. 1. Concept sketch of the coupled balloon wave energy converter.

It is of interest to evaluate how the CBWEC would perform in typical ocean wave conditions. To this end, this paper presents an analysis using a simplified model that considers the balloons to be ideal spheres pulsating uniformly in water. This approach is expected to give a conservative estimate of the device's performance.

Before proceeding with the analysis, we first present a brief review of similar pressure differential devices. Following [1], we define pressure differential devices as those that use wave-induced pressure differences to drive fluid flow, typically involving variable volumes that change with the flow.

II. Literature review

A. Pressure differential chambers

Pressure differential wave energy devices may trace their origin to Budal and Falnes [2], who presented a conceptual model of the coupled balloon resonator in 1974 (Fig. 2). The model consisted of two rigid air-filled tanks, enclosed at the top by flexible membranes (shown as dashed lines in the figure), designed to operate in pairs spaced at half a wavelength. Due to

Part of a special issue for ICOE 2024. Original version presented at ICOE 2024.

Manuscript submitted 18 June 2025; Accepted 30 June 2025. Published 13 April 2026.

This paper has been subject to single-blind peer review by a minimum of two reviewers.

This work was supported by Oceanworks, part of the FutureLab Network, through the RiverLab program, and by Marine Energy Research Australia (MERA), jointly funded by The University of Western Australia and the Western Australian Government, via the Department of Primary Industries and Regional Development (DPIRD).

B.-L. Chen was with The University of Western Australia, 35 Stirling Highway, Perth, WA 6009, Australia, and is now with Tailcon Projects, Perth, WA, Australia (e-mail: bolin.chen886@gmail.com)

A. Kurniawan, H. Wolgamot, and J. R. Whelan are with the School of Earth and Oceans, The University of Western Australia, 35 Stirling Highway, Perth, WA 6009, Australia (e-mails: adi.kurniawan@uwa.edu.au, hugh.wolgamot@uwa.edu.au).

Digital Object Identifier:
https://doi.org/10.36688/imej.8.449-457

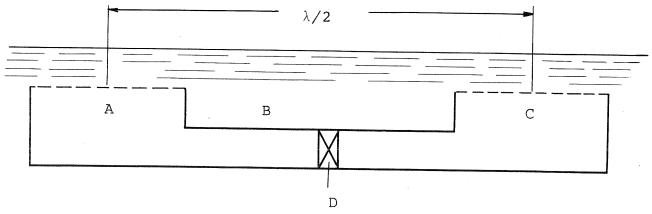

Fig. 2. Coupled balloon resonator proposed by Budal and Falnes, from [2].

wave forcing, the membranes alternately bulge in and out, resulting in a pumping action. A turbine converts the resulting pressure differential into useful energy. No theoretical analysis was presented.

A world patent for this idea was issued in 2013 under the name M3, and a scaled prototype was tested off the coast of Oregon in 2014 by M3 Wave LLC. A preliminary numerical analysis was conducted by McNatt et al. [1], who investigated the optimal length (or spacing between chambers) of such a device. Babarit et al. [3] analysed two versions of M3: one with the moving surface at the bottom (version 1), and the other with the moving surface at the top (version 2). They concluded that version 2 is more favourable for the ease of tuning its natural period (due to its negative hydrostatic stiffness) and its superior energy performance compared to a selection of other wave energy converters with various working principles. In both versions, the moving surface was a rigid horizontal plate, and this was accordingly assumed in their analysis. The analysis was extended in [4] to include surge, heave, and pitch of the system on a floating platform. It was found that the relative phase between pitch and the pumping mode is a key factor influencing the device's power performance. Coupling between pitch and the pumping mode can have positive effects on power production within certain wave frequency ranges.

In 2023, Milani et al. [5] investigated a coupled flexible membrane system using a setup comparable to Budal and Falnes' original concept—that is, with flexible membranes (rather than rigid surfaces) enclosing the chambers (see Fig. 3). Numerical predictions of the device's performance were partially validated through physical model tests in a wave flume. The findings reaffirmed the conclusions of Babarit et al. [3], highlighting the negative hydrostatic stiffness of the device and demonstrating that high power performance is achievable, provided additional (positive) stiffness is introduced to the system such that the membrane pumping motion resonates with the incident waves.

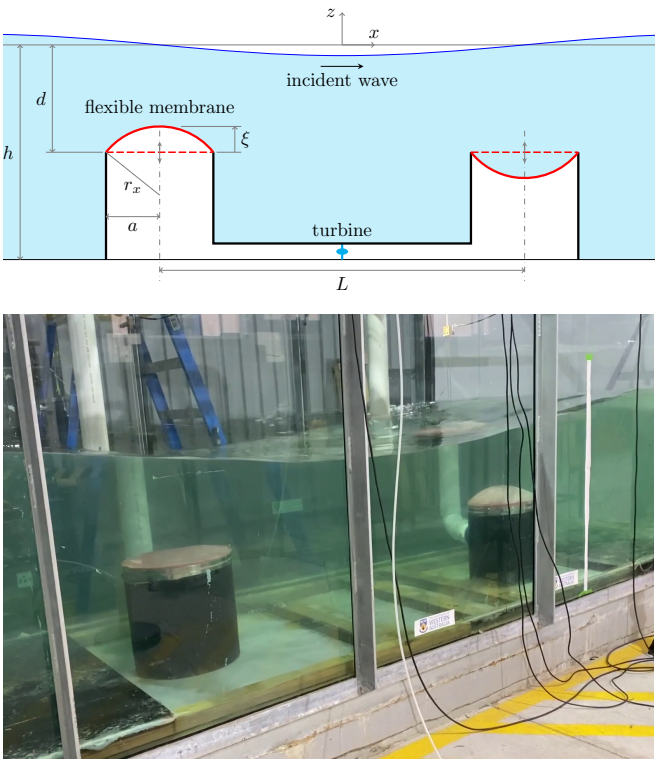

Fig. 3. Flexible-membrane wave energy device investigated in [5]: schematic (top) and photograph of the setup during model testing (bottom).

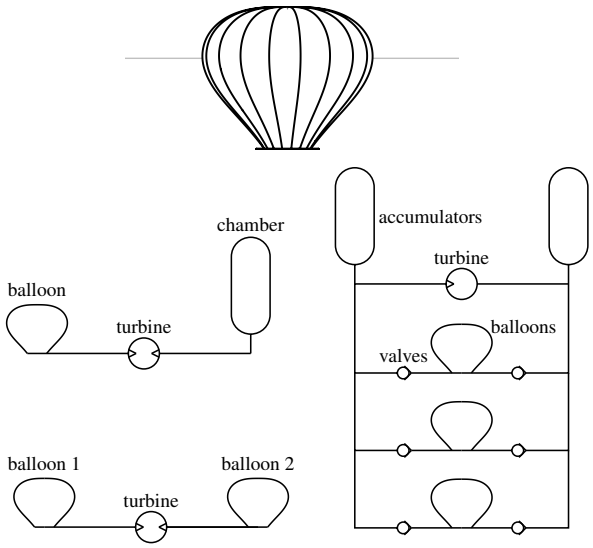

Fig. 4. Sketch of a seabed-fixed balloon (top) and possible configurations of the seabed-fixed balloon device (bottom). The single balloon connected to a fixed-volume chamber was considered in [6].

B. Seabed-fixed balloons

In 2016, Kurniawan and Greaves [6] investigated the performance of a single balloon attached to the seabed and connected to a fixed-volume chamber (Fig. 4). The balloon was constructed with tendons encasing the membrane, such that the balloon could deform but not stretch. The findings suggested that the single-balloon device might achieve more favourable power conversion if floating and heaving, or if coupled with another balloon, or operated in an array configuration (see Fig. 4). However, no analyses of these alternative configurations were presented.

C. Floating air bags

Following the study in [6], the authors further investigated the hydrodynamics of a floating, single air bag (Fig. 5). In this configuration, the fixed-volume chamber is housed within the device itself. The study concluded that the air bag exhibited a much longer heave resonance period than a rigid device, with only

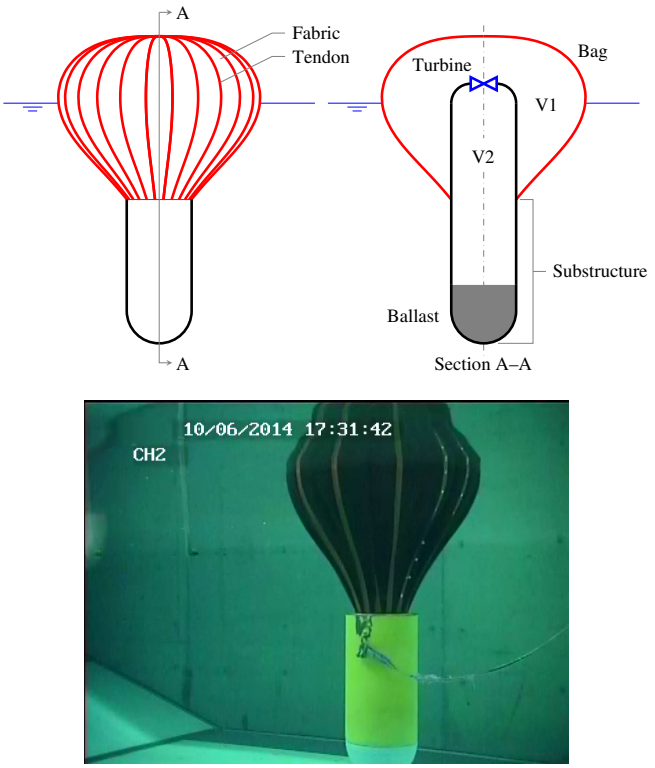

Fig. 5. Floating air bag WEC considered in [7]: sketch (top) and underwater view of a physical model (bottom).

a minor reduction in resonance bandwidth [7], [8]. This lengthening of the period (and corresponding reduction in bandwidth) arises from the compression of the bag during downward motion, which results in a lower restoring force (and correspondingly lower radiation capacity) compared to an equally sized rigid body. The increased natural period means that the air bag, as a wave energy device, can be significantly smaller than a rigid body with the same natural period.

D. Other devices

A number of other similar devices have been proposed in the literature.

One of the early devices to utilise pressure differential to generate air flow is the flexible bag device proposed by French [9]. The device comprises multiple air-filled flexible bags mounted on a long floating platform oriented along the wave direction. The passage of waves along the platform drives the bags to expand and contract, creating air flow which is utilised for power generation via an air turbine. Bombora [10] is a relatively recent concept utilising the same principle, but is bottom-fixed and completely submerged.

Righi et al. [11] considered a single chamber with a direct-drive dielectric elastomer generator (DEG) as the power take-off (PTO), removing the need for a turbine. Capitalising on the negative hydrostatic stiffness property of an upward-facing moving surface [12], the device consists of a submerged air chamber with a deformable DEG enclosing the top. Thus, the DEG acts both as a deformable interface between air and water, and as a PTO.

Other pressure-differential devices include the Archimedes Wave Swing (AWS) [13], which consists of an air-filled chamber fixed to the seabed and a cylindrical lid that moves vertically. Further development of this concept led to Symphony, a variable-volume submerged point absorber [14], [15]. An array of similar devices has also been considered in hybrid configuration with a floating wind turbine [16].

III. Simplified Model

An interesting feature of pressure-differential devices of the type considered here is that their natural periods are non-trivial, as demonstrated by Milani et al. [5]. The stiffness of the pumping mode comprises hydrostatic, pneumatic, and any additional contributions, such as membrane stiffness. Moreover, the pneumatic stiffness is frequency-dependent and influenced by the flow resistance between the two chambers.

A. Assumptions

In this preliminary study, we consider two identical pulsating spheres as shown in Fig. 6 as an idealised model of the proposed CBWEC (in fact, a submerged balloon in a hydrostatic pressure field does not adopt a spherical shape). Each sphere is of mean radius a and is assumed to expand/contract uniformly. The centres of the spheres are fixed in place, that is, we assume that there are no motions other than the pulsation of the spheres.

We define a global coordinate system with the origin at the mean free surface, midway between the two spheres. The x-axis points along the incident wave direction and the z-axis points upward. For sphere m, we also define a local coordinate system with origin at the centre of the sphere and axes parallel to the global axes. The unit normal vector $\mathbf{n}$ is defined as pointing out of the body.

We assume that all oscillations are small and time-harmonic so that any oscillating quantity $x(t)$ can be written as $x(t) = \mathrm{Re}\{x\mathrm{e}^{-\mathrm{i}\omega t}\}$, where x is the complex amplitude (the minus sign in the $-\mathrm{i}\omega t$ time dependence is chosen in agreement with the convention used in HydroStar [17], which is used to compute the hydrodynamic coefficients).

B. Mode definition

We define two modes to describe the motion of the spheres. Mode I is in-phase expansion/contraction of both spheres. Mode II is anti-phase (sphere 1 contracts, sphere 2 expands). No other motions are allowed. Following Newman [18], we define the shape function $\mathbf{S}_i$ of mode i as the displacement of a point on the body for a unit modal displacement ξ_i. Thus, for sphere m,

$$\mathbf{S}_I = (x_m\mathbf{i} + y_m\mathbf{j} + z_m\mathbf{k})/a, \tag{1}$$

$$\mathbf{S}_{II} = (-1)^m(x_m\mathbf{i} + y_m\mathbf{j} + z_m\mathbf{k})/a. \tag{2}$$

Alternatively, we could use the expansion of one individual sphere (while holding the other one fixed) as one mode, such as used in [5], but the advantage of using symmetric and antisymmetric modes is that they lead to uncoupled equations of motion.

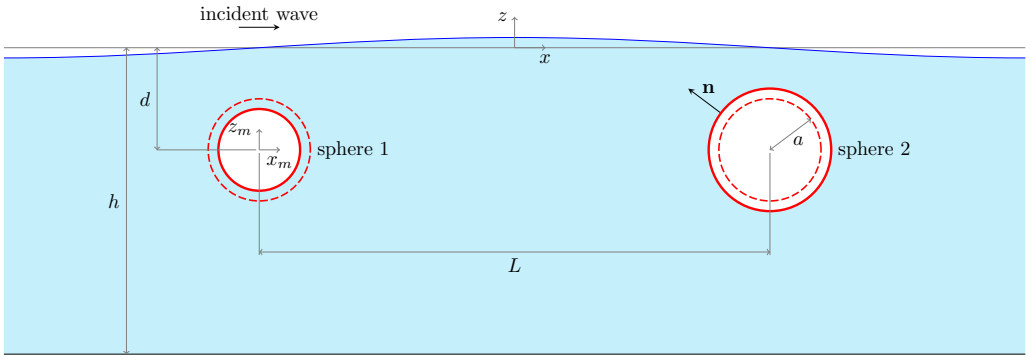

Fig. 6. The coupled balloon device as two pulsating spheres, with notation.

The local and global coordinates (see Fig. 6) are related as

$$x_1 = x + L/2, \tag{3}$$
$$x_2 = x - L/2, \tag{4}$$
$$y_1 = y_2 = y, \tag{5}$$
$$z_1 = z_2 = z + d. \tag{6}$$

Using relations (3)–(6), we may rewrite the shape functions (1) and (2) in terms of the global coordinates:

$$\mathbf{S}_I = \frac{1}{a}\left\{\left[x + (-1)^{m-1}\frac{L}{2}\right]\mathbf{i} + y\mathbf{j} + (z+d)\mathbf{k}\right\}, \tag{7}$$
$$\mathbf{S}_{II} = \frac{(-1)^m}{a}\left\{\left[x + (-1)^{m-1}\frac{L}{2}\right]\mathbf{i} + y\mathbf{j} + (z+d)\mathbf{k}\right\}. \tag{8}$$

C. Hydrostatics

The elements of the hydrostatic stiffness matrix $\mathbf{K}$ can be obtained from the shape functions following [18]:

$$K_{ij} = -\rho g \int_{S_b} n_j(w_i + zD_i)\mathrm{d}S, \tag{9}$$

where w_j is the z-component of the shape function, $n_j = \mathbf{S}_j \cdot \mathbf{n}$ is the normal component, and $D_j = \nabla \cdot \mathbf{S}_j$ is the divergence. The integral is taken over the wetted body surface S_b.

Knowing the shape functions and the geometry of the body, we can evaluate w_j, n_j, and D_j. The z-component of the shape functions are

$$w_I = (z+d)/a, \tag{10}$$
$$w_{II} = (-1)^m(z+d)/a \quad \text{for sphere } m, \tag{11}$$

the normal components are

$$n_I = 1, \tag{12}$$
$$n_{II} = (-1)^m \quad \text{for sphere } m, \tag{13}$$

and the divergences are

$$D_I = 2/a, \tag{14}$$
$$D_{II} = 2(-1)^m/a \quad \text{for sphere } m. \tag{15}$$

To evaluate the integral (9), it is convenient to use spherical coordinates. Denoting the azimuthal angle as θ and the polar angle as ϕ, on the sphere surface we have

$$x = a\sin\phi\cos\theta \mp L/2, \tag{16}$$
$$y = a\sin\phi\sin\theta, \tag{17}$$
$$z = a\cos\phi - d, \tag{18}$$
$$\mathrm{d}S = a^2\sin\phi\,\mathrm{d}\phi\,\mathrm{d}\theta. \tag{19}$$

With these, we obtain

$$K_{I,I} = 16\rho g\pi a d, \tag{20}$$
$$K_{II,II} = K_{I,I}, \tag{21}$$
$$K_{I,II} = K_{II,I} = 0. \tag{22}$$

We note that this is simply the linearised rate of change in buoyancy force, $2 \times 4\pi[(a+\xi_i)^2 - a^2]\rho g d$, with displacement ξ_i.

D. Pneumatic forces

The relationship between pressure, volume, and mass increases in sphere m is obtained by linearising the isentropic equation. The result is

$$\frac{V_m}{V_0} = \frac{m_m}{m_0} - \frac{p_m}{\gamma p_0}, \tag{23}$$

where V_0 is the mean volume of each sphere, m_0 is the mean air mass in each sphere, assumed to be equal to $\rho_{\text{air}}V_0$ (where ρ_{air} is the mean air density), p_0 is the mean air pressure including the atmospheric pressure p_{atm}, and γ is the heat capacity ratio.

The mass flow through the turbine is assumed to be linearly proportional to the pressure difference between the two spheres, with c being the linear power take-off coefficient:

$$\mathrm{i}\omega m_1 = -\mathrm{i}\omega m_2 = c(p_1 - p_2). \tag{24}$$

Larger c means smaller flow resistance.

Substituting (24) into (23), we obtain

$$\begin{pmatrix} V_1 \\ V_2 \end{pmatrix} = \begin{pmatrix} A_V & A_c \\ A_c & A_V \end{pmatrix}\begin{pmatrix} p_1 \\ p_2 \end{pmatrix}, \tag{25}$$

where

$$A_V = -\frac{V_0}{\gamma p_0} - \frac{c}{\omega\rho_{\text{air}}}\mathrm{i}, \tag{26}$$
$$A_c = \frac{c}{\omega\rho_{\text{air}}}\mathrm{i}. \tag{27}$$

At this point, it is useful to define $\xi_m, m = 1, 2$ as the displacement of each sphere in the normal direction (expansion). The modal displacements ξ_I and ξ_{II} are therefore related to the sphere displacements ξ_1 and ξ_2 as

$$\xi_I - \xi_{II} = \xi_1, \tag{28}$$

$$\xi_I + \xi_{II} = \xi_2. \tag{29}$$

The linearised volume increase of sphere m after displacement ξ_m is

$$V_m = 4\pi a^2 \xi_m. \tag{30}$$

The increase in air pressure in the spheres creates a force on the sphere. In the j-direction, this force is given as

$$F_{p,j} = \int_{S_b} p n_j \mathrm{d}S. \tag{31}$$

This gives

$$\begin{pmatrix} F_{p,I} \\ F_{p,II} \end{pmatrix} = 4\pi a^2 \mathbf{L} \begin{pmatrix} p_1 \\ p_2 \end{pmatrix}, \tag{32}$$

where

$$\mathbf{L} = \begin{pmatrix} 1 & 1 \\ -1 & 1 \end{pmatrix}. \tag{33}$$

Combining (25)–(32), we obtain

$$\begin{aligned} \begin{pmatrix} F_{p,I} \\ F_{p,II} \end{pmatrix} &= 16\pi^2 a^4 \mathbf{L} \begin{pmatrix} A_V & A_c \\ A_c & A_V \end{pmatrix}^{-1} \mathbf{L}^\intercal \begin{pmatrix} \xi_I \\ \xi_{II} \end{pmatrix} \\ &= \underbrace{32\pi^2 a^4 \begin{pmatrix} \dfrac{1}{A_V + A_c} & 0 \\ 0 & \dfrac{1}{A_V - A_c} \end{pmatrix}}_{\equiv \mathbf{G}} \begin{pmatrix} \xi_I \\ \xi_{II} \end{pmatrix}, \end{aligned} \tag{34}$$

which relates the pneumatic forces to the modal displacements.

E. Additional stiffness

We assume in general that there is an additional stiffness that resists the expansion and contraction of each sphere, such that the additional restoring force is

$$F_{a,m} = -k_a \xi_m, \tag{35}$$

where k_a is the additional stiffness coefficient.

Like the pneumatic forces, this can be expressed in terms of modes I and II:

$$\begin{aligned} \begin{pmatrix} F_{a,I} \\ F_{a,II} \end{pmatrix} &= -k_a \mathbf{L}\mathbf{L}^\intercal \begin{pmatrix} \xi_I \\ \xi_{II} \end{pmatrix} \\ &= -\underbrace{2k_a \begin{pmatrix} 1 & 0 \\ 0 & 1 \end{pmatrix}}_{\equiv \mathbf{K}_a} \begin{pmatrix} \xi_I \\ \xi_{II} \end{pmatrix}. \end{aligned} \tag{36}$$

F. Hydrodynamic forces

The added mass, radiation damping, and exciting forces associated with the two modes I and II are evaluated from HydroStar using the generalised mode option. This is done by specifying the displacement of every panel according to the shape functions (1)–(2).

G. Equations of motion

Assembling all the forcing terms, we arrive at the following equations of motion:

$$\left[-\omega^2 \mathbf{M}_r - \mathrm{i}\omega \mathbf{R}_r + \mathbf{K} + \mathbf{K}_a - \mathbf{G}\right] \boldsymbol{\xi} = \mathbf{F}_e, \tag{37}$$

where $\mathbf{M}_r$, $\mathbf{R}_r$, and $\mathbf{F}_e$ are the added mass, radiation damping, and excitation force calculated from HydroStar, $\mathbf{K}$ is the hydrostatic stiffness matrix whose elements are given in (20)–(22), $\mathbf{K}_a$ is the additional stiffness matrix given in (36), and $\mathbf{G}$ is the complex matrix given in (34). The mass of the surface of the sphere is assumed to be negligible.

Equation (37) can be solved for the modal displacements $\boldsymbol{\xi} = \begin{pmatrix} \xi_I & \xi_{II} \end{pmatrix}^\intercal$, from which the pressure amplitudes in the spheres can be obtained from (25)–(30). Knowing the pressures, we can in turn calculate the absorbed power from

$$P = \frac{c}{2\rho_{\mathrm{air}}} |p_1 - p_2|^2. \tag{38}$$

We note that all terms on the left-hand side of (37) are diagonal matrices, meaning that the two equations are uncoupled and can be solved individually.

IV. Generalisation to partial submergence

It is straightforward to generalise the preceding analysis to include cases where the spheres are piercing the free surface. We can show that, for arbitrary submergence,

$$K_{I,I} = \begin{cases} 2\rho g \pi (a+d)(3a+d) & \text{for } -a \le d \le a \\ 16 \rho g \pi a d & \text{for } a < d < h - a, \end{cases} \tag{39}$$

while (21)–(22) remain valid. Here, $d < 0$ means that the centre of the sphere is above the mean free surface. Further, denoting the factor $4\pi a^2$ in (32) by s, we can show that

$$s = \begin{cases} 2\pi a (a+d) & \text{for } -a \le d \le a \\ 4\pi a^2 & \text{for } a < d < h - a, \end{cases} \tag{40}$$

such that the factor $32\pi^2 a^4$ in matrix $\mathbf{G}$ is valid for $a < d < h - a$, but becomes $16\pi^2 a^3 (a+d)$ for $-a \le d \le a$. These are the only changes to the equations.

V. Performance

To evaluate the performance of the device, we consider all possible combinations of dimensions listed in Table I. Performance is assessed by integrating the absorbed power function over wave periods, assigning equal weight to all periods. We refer to this quantity as the *potential power*. The dimensions in the table are selected to represent a possible full-scale device, and Fig. 6 is a sketch to scale, corresponding to $h = 30$ m, $d = 10$ m, $L = 50$ m, and $a = 5$ m.

The added mass, radiation damping, and excitation force coefficients corresponding to the two defined modes are plotted in Fig. 7 for the case with $L = 50$ m, $d = 10$ m, and $p_0 - p_{\mathrm{atm}} = 10$ m (of water). The off-diagonal added mass and radiation damping coefficients are zeros, as expected, since the two modes are uncoupled. When $L = (n - 1/2)\lambda$, $n = 1, 2, \ldots$, the

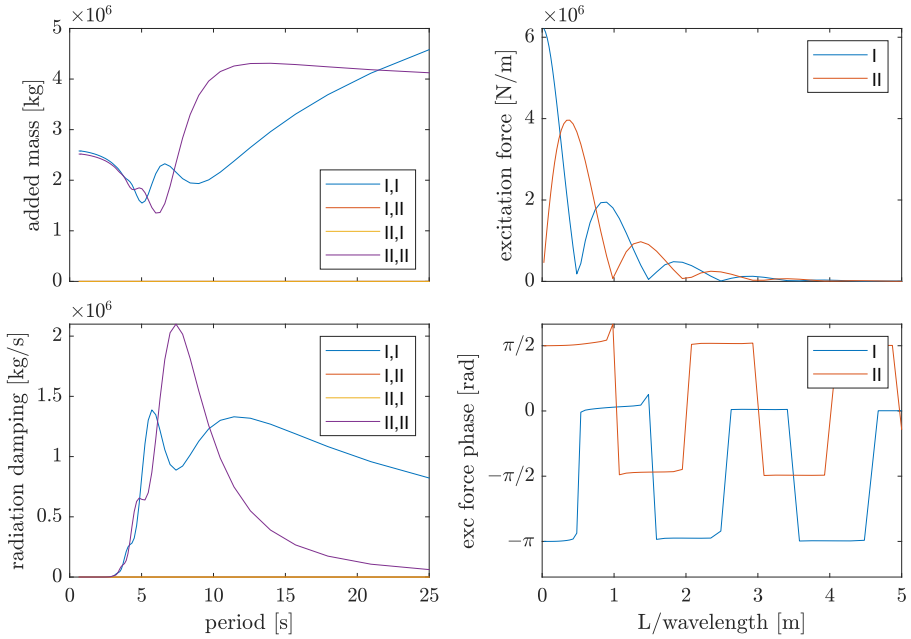

Fig. 7. Added mass, radiation damping, excitation force coefficients, and the phase of the excitation force, for $a = 5$ m, $L = 50$ m, $d = 10$ m, $h = 30$ m, and $p_0 - p_{\text{atm}} = 10$ m (of water).

TABLE I
DEVICE DIMENSIONS AND PARAMETERS ASSUMED IN THE MODEL

Parameter	Notation	Value
Radius [m]	a	5
Centre-to-centre spacing [m]	L	30, 40, 50
Centre submergence [m]	d	0, 2.5, 6.25, 7.5, 10, 22.5
Water depth [m]	h	30
Mean pressure [m of water]	$p_0 - p_{\text{atm}}$	0, 2.5, 6.25, 7.5, 10, 22.5
Air density [kg/m^3]	ρ_{air}	1.2
Heat capacity ratio	γ	1.4

excitation force for the symmetric (in-phase) mode is (almost) cancelled, while the excitation force for the anti-symmetric (anti-phase) mode is maximised. For $n = 1$, this corresponds to $\lambda = 2L = 100$ m, or $T = 8$ s for the given water depth, and the period also aligns with the peak of typical wave energy spectra. Conversely, when $L = n\lambda$, $n = 1, 2, \ldots$, the excitation force for the anti-symmetric mode is (almost) cancelled, while that for the symmetric mode is maximised. Note, however, that the peaks of the excitation force for one mode do not align exactly with the zeros of the other mode but occur at slightly longer wavelengths, due to diffraction effects.

While typical floating WECs generally have better capabilities for absorbing wave power, a focus on fully submerged devices is emphasised to highlight the original idea of a fully-submerged device.

As an example, the displacement and pressure amplitude of each sphere, as well as the absorbed power, for $L = 50$ m, $d = 6.25$ m, and $\rho_{\text{air}}/c = 238.6$ kg m^{-4} s^{-1}, are plotted in Fig. 8, left column. This gives a potential power of 1.81 MJ m^{-2}, which is about the best achievable for this submergence level, with no additional stiffness ($k_a = 0$). Although the power function is broad-banded, it is rather low compared to the theoretical limits. However, if k_a is negative, significantly more power can be absorbed (Fig. 8, right column). In this case, the natural period T_n of the anti-symmetric mode is tuned to match the wave period by adjusting both k_a and ρ_{air}/c. By setting the maximum T_n to 8 s, an optimal combination of k_a and ρ_{air}/c can be found to maximise the potential power. For a device with $L = 50$ m and greater submergence depth ($d = 10$ m), the optimal parameters are $k_a = -11.7$ MN/m and $\rho_{\text{air}}/c = 25.4$ kg m^{-4} s^{-1}. The potential power increases substantially to 15.8 MJ m^{-2}—almost nine times that of the previous case, which has no additional (negative) stiffness.

The presence or absence of additional stiffness leads to different power take-off requirements to achieve optimal performance, as shown in Table II.

The behaviour of a well-tuned device is generally similar to that of the submerged membrane device studied by Milani et al. [5].

Decreasing the spacing between the balloons is found to reduce the potential power roughly proportionally.

VI. DISCUSSION AND CONCLUSIONS

This section discusses the key findings of the analysis, their implications for design, and possible directions for improving the performance and practicality of the proposed coupled balloon wave energy converter (CBWEC). Limitations of the current model and plans for experimental validation are also outlined.

Our analysis, based on a simplified model in which the balloons are treated as ideal pulsating spheres, suggests that good power absorption is achievable in a fully submerged configuration—provided that negative stiffness is introduced into the system. The need for negative stiffness arises because the fully submerged device is otherwise too stiff in the pumping

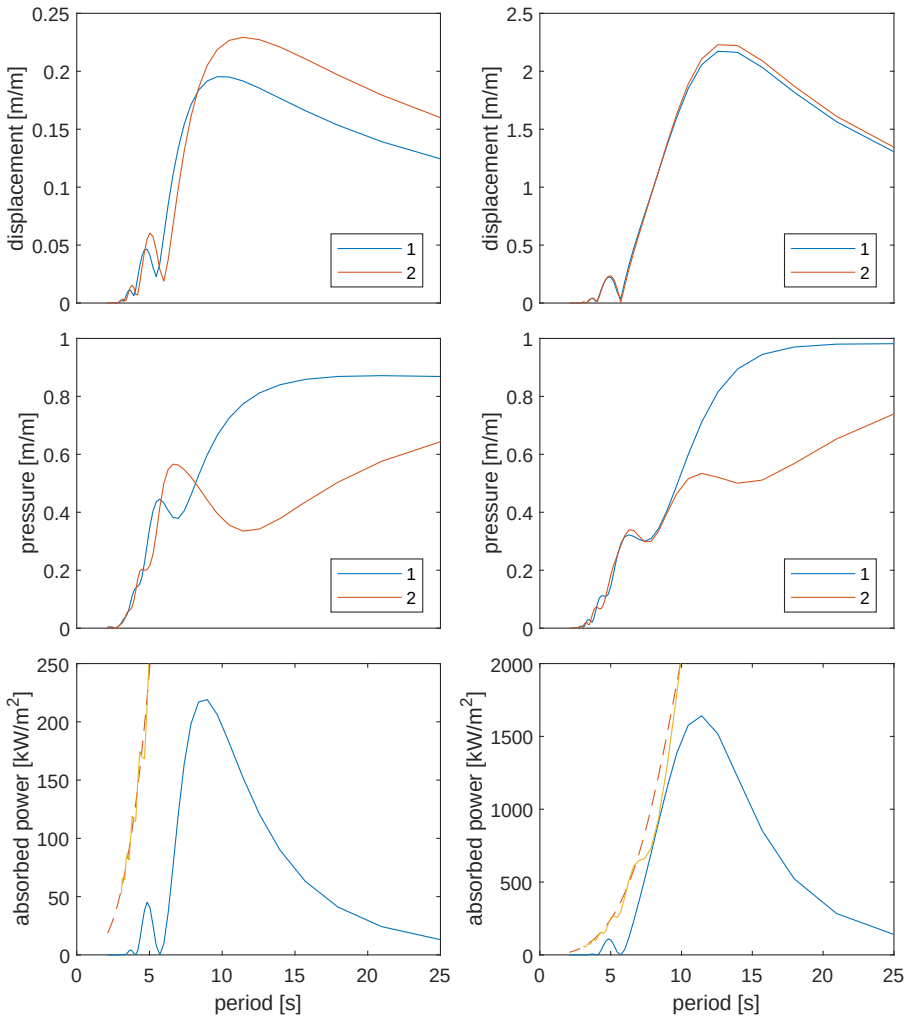

Fig. 8. Displacements, pressure amplitudes, and absorbed power, per unit incident wave amplitude, for $k_a = 0$ N/m, $d = 6.25$ m, and $\rho_a/c = 238.6$ kg m^{-4} s^{-1} (left) and $k_a = -1.174 \times 10^7$ N/m, $d = 10$ m, and $\rho_a/c = 25.4$ kg m^{-4} s^{-1} (right). For the absorbed power functions (bottom plots), the ascending solid line shows the maximum theoretical limit for the given geometry, and the ascending dashed line shows the maximum theoretical limit for a dipole.

mode and does not resonate with typical ocean wave periods. While the use of negative stiffness enables resonance and enhances performance, its practical implementation may be challenging. Negative stiffness has been studied in other contexts, such as shock absorption [19], and similar ideas—such as embedding a honeycomb structure within the balloons—may be worth exploring.

Instead of fully submerging the balloons, allowing them to pierce the free surface (i.e., be half-submerged) reduces the hydrostatic stiffness to a level that—while still insufficient to achieve resonance—enables appreciable power absorption even without the introduction of negative stiffness. In Table II, this corresponds to the cases with $d = 0$ and $k_a = 0$. The highest potential power in this configuration is 3.09 MJ m^{-2}, achieved with $L = 50$ m. This is about one-fifth of the highest potential power obtained in the fully-submerged case with negative k_a.

The present model is idealised. A natural next step would be to extend the analysis to account for more realistic mean shapes and deformations of the balloons. This is expected to alter both the hydrostatic and hydrodynamic properties of the system, although—depending on the construction of the balloons—it is not immediately clear whether the effect will be beneficial or detrimental.

Various practical modifications could improve the CBWEC's performance. One approach is to apply latching control [20] to artificially lengthen the device's natural period. This could be implemented using a valve between the balloons that opens only during certain parts of the wave cycle—e.g., when a wave crest or trough passes over a balloon—and remains closed otherwise. Such a strategy would achieve a similar effect to that of introducing negative stiffness, though the impact of transient pressure fluctuations on balloon performance would need to be considered.

Another possibility is to allow the balloons to heave, for example using a pulley mechanism. This additional degree of freedom would reduce the effective stiffness of the pumping mode and thus improve performance. However, the system may become statically unstable, with one balloon rising while the other sinks. An end-stop mechanism could be introduced to limit the rise and fall of the balloons.

In practical deployment, the balloons may also swing like inverted pendulums. The natural period of this

TABLE II
OPTIMAL PARAMETERS FOR SELECTED CONFIGURATIONS

$L = 50$ m					
d [m]	$k_a = 0$		$k_a < 0$		
	ρ_{air}/c [kg m^{-4} s^{-1}]	potential power [MJ m^{-2}]	ρ_{air}/c [kg m^{-4} s^{-1}]	k_a [MN m^{-1}]	potential power [MJ m^{-2}]
0	134	3.09	27.2	-1.87	18.3
2.5	163	2.46	33.1	-3.31	14.4
6.25	239	1.81	37.4	-6.69	13.7
7.5	297	1.32	31.3	-8.43	14.8
10	418	0.809	25.4	-11.7	15.8
22.5	1080	0.216	26.1	-27.5	11.0
$L = 40$ m					
d [m]	$k_a = 0$		$k_a < 0$		
	ρ_{air}/c [kg m^{-4} s^{-1}]	potential power [MJ m^{-2}]	ρ_{air}/c [kg m^{-4} s^{-1}]	k_a [MN m^{-1}]	potential power [MJ m^{-2}]
0	118	2.56	24.2	-1.84	14.1
2.5	144	2.03	30.4	-3.24	10.9
6.25	213	1.50	38.9	-6.48	9.52
7.5	267	1.07	32.0	-8.26	10.3
10	380	0.628	25.1	-11.6	11.0
22.5	1020	0.153	22.3	-27.4	7.93
$L = 30$ m					
d [m]	$k_a = 0$		$k_a < 0$		
	ρ_{air}/c [kg m^{-4} s^{-1}]	potential power [MJ m^{-2}]	ρ_{air}/c [kg m^{-4} s^{-1}]	k_a [MN m^{-1}]	potential power [MJ m^{-2}]
0	101	1.96	18.9	-1.84	10.8
2.5	125	1.55	24.4	-3.24	8.28
6.25	187	1.14	33.8	-6.41	6.86
7.5	235	0.785	27.5	-8.21	7.34
10	341	0.437	20.8	-11.6	7.79
22.5	975	0.0950	17.2	-27.4	5.32

swinging motion is approximately

$$T_n \approx 2\pi\sqrt{\frac{h-d}{2g}}, \tag{41}$$

where h and d are defined in Fig. 6. For $h = 30$ m and $d = 10$ m, this yields a swing natural period of 6.3 s. To avoid resonance with this swinging motion, it may be advisable to limit the operational water depth to less than 30 m.

Experimental validation of the CBWEC model is planned in the near future through physical testing in the wave flume at the Coastal and Offshore Research Laboratory, The University of Western Australia. These tests will help confirm the validity of the analysis and may provide additional insights not captured in the simplified model.

Finally, the practical suitability of membrane materials for wave energy applications—relevant to the construction of the balloons—has been comprehensively reviewed by Collins et al. [21]. Their findings offer valuable guidance for future development of the device.

REFERENCES

[1] J. C. McNatt, H. T. Özkan Haller, M. Morrow, and M. Delos-Reyes, "Preliminary modeling and analysis of a horizontal pressure differential wave energy converter," *Journal of Offshore Mechanics and Arctic Engineering*, vol. 136, no. 1, Nov 2014.

[2] K. Budal and J. Falnes, "Proposals for conversion of the energy in ocean waves," Institutt for eksperimentalfysikk, NTH, Tech. Rep., March 1974.

[3] A. Babarit, F. Wendt, Y.-H. Yu, and J. Weber, "Investigation on the energy absorption performance of a fixed-bottom pressure-differential wave energy converter," *Applied Ocean Research*, vol. 65, pp. 90–101, 2017.

[4] F. Wendt, Y.-H. Yu, A. Babarit, and M. Delos-Reyes, "Numerical analysis and validation of a pressure-differential wave energy converter," in *Proceedings of the 4th Asian Wave and Tidal Energy Conference*, Taipei, Taiwan, 2018.

[5] L. Milani, S. Thorniley, A. Kurniawan, and H. Wolgamot, "Modelling and testing of a pressure-differential wave energy converter with flexible membranes," *Applied Ocean Research*, vol. 134, p. 103516, 2023.

[6] A. Kurniawan and D. Greaves, "Wave power absorption by a submerged balloon fixed to the sea bed," *IET Renewable Power Generation*, vol. 10, no. 10, pp. 1461–1467, 2016.

[7] A. Kurniawan, J. R. Chaplin, D. M. Greaves, and M. Hann, "Wave energy absorption by a floating air bag," *Journal of Fluid Mechanics*, vol. 812, pp. 294–320, 2017.

[8] A. Kurniawan, S. Brown, D. Forehand, and H. Wolgamot, "Wave-structure interactions of flexible bags with elastic tendons: Application to wave energy conversion," *Journal of Waterway, Port, Coastal, and Ocean Engineering*, vol. 147, no. 1, p. 04020045, 2021.

[9] M. J. French, "The search for low cost wave energy and the flexible bag device," in *Proc 1st Int Symp Wave Energy Util*, Gothenburg, Sweden, 1979, pp. 364–377.

[10] C. Algie, S. Ryan, and A. Fleming, "Predicted power performance of a submerged membrane pressure-differential wave energy converter," *International Journal of Marine Energy*, vol. 20, pp. 125–134, 2017.

[11] M. Righi, G. Moretti, D. Forehand, L. Agostini, R. Vertechy, and M. Fontana, "A broadbanded pressure differential wave energy converter based on dielectric elastomer generators," *Nonlinear Dynamics*, vol. 105, no. 4, pp. 2861–2876, Sep 2021.

[12] A. Kurniawan, D. Greaves, and J. Chaplin, "Wave energy devices with compressible volumes," *Proceedings of the Royal Society A: Mathematical, Physical and Engineering Sciences*, vol. 470, no. 2172, p. 20140559, 2014.

[13] M. G. de Sousa Prado, F. Gardner, M. Damen, and H. Polinder, "Modelling and test results of the Archimedes Wave Swing,"

Proceedings of the Institution of Mechanical Engineers, Part A: Journal of Power and Energy, vol. 220, no. 8, pp. 855–868, 2006.

[14] J. M. van der Jagt, "A methodology for assessing power performance, applied to a quasi-rigid submerged pressure differential device," Master Thesis, TU Delft, 2018.

[15] J. Candido, A. Sarmento, F. E. Gardner, L. M. Gato, M. Fontana, and K. M. Collins, "The WETFEET project - A disruptive approach to wave energy," in *Proceedings of the 13th European Wave and Tidal Energy Conference*, Naples, Italy, 2019.

[16] N. McLean, E. Bannon, M. Holland, D. Forehand, T. Giles, K. Smith, and T. Davey, "Multi wave absorber platform design, modelling and testing: Investigating the integration of multiple wave energy absorbers into a floating offshore wind platform considering a future wind and wave energy hybrid system," in *Proceedings of the 15th European Wave and Tidal Energy Conference*, vol. 15, Bilbao, Spain, 2023.

[17] B. Veritas, *HydroStar for Experts: User Manual*, Bureau Veritas, 92571 Neuilly-Sur-Seine, April 2021, v8.10.

[18] J. Newman, "Wave effects on deformable bodies," *Applied Ocean Research*, vol. 16, no. 1, pp. 47–59, 1994.

[19] D. M. Correa, C. C. Seepersad, and M. R. Haberman, "Mechanical design of negative stiffness honeycomb materials," *Integrating Materials and Manufacturing Innovation*, vol. 4, pp. 165–175, 2015.

[20] J. Falnes, "Optimum control of oscillation of wave-energy converters," in *The Eleventh International Offshore and Polar Engineering Conference*, Stavanger, Norway, 2001.

[21] I. Collins, M. Hossain, W. Dettmer, and I. Masters, "Flexible membrane structures for wave energy harvesting: A review of the developments, materials and computational modelling approaches," *Renewable and Sustainable Energy Reviews*, vol. 151, p. 111478, 2021.